

Formulation and Numerical Post-bifurcation Analysis of Frictional Dilatant Materials at Finite Strains

Keisuke Satoh¹, Yuki Yamakawa¹, Yasuyuki Miyaki¹, Kunio Torii¹

Summary

This paper presents a formulation and numerical analysis for bifurcation in frictional dilatant materials like geomaterials at finite strains. The Cauchy stress is employed to represent the yield function in place of the Kirchhoff stress which is often used in metal plasticity. The energy-conserving elasticity and the non-associative format of the plastic flow rule, together with the non-symmetric tangent moduli, are naturally derived. We extend numerical scheme for bifurcation analysis to problems in which the tangent stiffness matrix of FE-discretized system is non-symmetric. Some numerical examples of bifurcation analyses are demonstrated.

Introduction

The development of computational model for finite strains in recent years has made mathematical structure of plasticity theory more clear and has provided efficient numerical schemes. In this paper the importance of the choice of the stress measure in the expression of yield functions at finite strains is emphasized in view of the relation between modeling of materials and calibration through experiments.

A basic kinematic concept of the multiplicative decomposition of the deformation gradient is adapted to model materials at finite strains. While the yield function for metal plasticity is often expressed in terms of the Kirchhoff stress, it is pointed out by Meschke et al. [1] that, for isotropic frictional dilatant materials such as geomaterials, the Cauchy stress might be more suitable to represent the yield function. In this case the spatial format of the dissipation inequality and the principle of maximum dissipation naturally lead to the energy-conserving elasticity and the non-associative format of the plastic flow rule. Due to this non-associativity of the plastic flow rule, the material tangent modulus loses its symmetry.

We extend the scheme for numerical bifurcation analysis to problems in which the tangent stiffness matrix of the system does not possess the symmetry[2]. Some numerical examples for post-bifurcation behavior of plane strain specimens under uniform compression are presented. As a model of geomaterials, a perfectly-plastic Drucker–Prager model with associated/non-associated flow rule is employed. A significant role of bifurcation in the occurrence of typical failure modes is demonstrated through the numerical bifurcation analysis.

¹Department of Civil and Environmental Engineering, Nagaoka University of Technology, Nagaoka 940-2188, Japan.

Formulations of Material Models and Boundary Value Problem at Finite Strains

A basic kinematic assumption of the multiplicative decomposition of the deformation gradient into elastic and plastic parts $\mathbf{F} = \mathbf{F}^e \cdot \mathbf{F}^p$ is considered. The elastic left Cauchy–Green deformation tensor and its rate are respectively given as

$$\mathbf{b}^e = \mathbf{F}^e \cdot \mathbf{F}^{eT}, \quad \dot{\mathbf{b}}^e = \mathbf{l} \cdot \mathbf{b}^e + \mathbf{b}^e \cdot \mathbf{l}^{eT} + \mathcal{L}_v \mathbf{b}^e, \quad (1)$$

where $\mathbf{l} = \dot{\mathbf{F}} \cdot \mathbf{F}^{-1}$ is the spatial velocity gradient, $\mathcal{L}_v \mathbf{b}^e = \mathbf{F} \cdot [\partial(\mathbf{F}^{-1} \cdot \mathbf{b}^e \cdot \mathbf{F}^{-T}) / \partial t] \cdot \mathbf{F}^T$ is the Lie derivative of \mathbf{b}^e , and $\partial(\cdot) / \partial t$ denotes the material time derivative. The velocity gradient \mathbf{l} can be additively decomposed into elastic and plastic parts as

$$\mathbf{l} = \mathbf{l}^e + \mathbf{l}^p, \quad \mathbf{l}^e = \dot{\mathbf{F}}^e \cdot (\mathbf{F}^e)^{-1}, \quad \mathbf{l}^p = \mathbf{F}^e \cdot \bar{\mathbf{L}}^p \cdot (\mathbf{F}^e)^{-1}, \quad (2)$$

where $\bar{\mathbf{L}}^p = \dot{\mathbf{F}}^p \cdot (\mathbf{F}^p)^{-1}$ is the plastic part of the velocity gradient on the plastically deformed configuration associated with \mathbf{F}^p , and \mathbf{l}^p is the push-forward of $\bar{\mathbf{L}}^p$ to the current configuration. In what follows, we employ a constitutive assumption for the plastic spin $\mathbf{w}^p = \text{skw}[\mathbf{l}^p] = \mathbf{0}$.

Assuming isotropic hyperelasticity, we can express the free energy function Ψ as a function of \mathbf{b}^e via its invariants (not \mathbf{b}^e itself). Restricting to the case of isotropic hardening, we introduce a strain-ordered internal variable κ , which is work conjugate to a stress-ordered variable k . With these notations in hand, the rate of dissipation \mathcal{D} per unit reference volume can be expressed in reduced form

$$\mathcal{D} = \boldsymbol{\tau} : \mathbf{d} - \dot{\Psi}(\mathbf{b}^e, \kappa) = \boldsymbol{\tau} : \left[-\frac{1}{2}(\mathcal{L}_v \mathbf{b}^e) \cdot (\mathbf{b}^e)^{-1} \right] + k\dot{\kappa} \geq 0, \quad (3)$$

where $\boldsymbol{\tau}$ is the Kirchhoff stress, $\mathbf{d} = \text{sym}[\mathbf{l}]$ is the spatial rate of deformation. The hyperelastic constitutive relation and the isotropic hardening law emerge as

$$\boldsymbol{\tau} (= J\boldsymbol{\sigma}) = 2 \frac{\partial \Psi}{\partial \mathbf{b}^e} \cdot \mathbf{b}^e, \quad k = -\frac{\partial \Psi}{\partial \kappa}, \quad (4)$$

where $J = \det \mathbf{F}$ represents the volume change, and $\boldsymbol{\sigma}$ is the Cauchy stress. In contrast to usual treatments for plastic incompressible materials, we here express the yield function of frictional dilatant materials like soils in terms of the Cauchy stress $\boldsymbol{\sigma}$ as $f(\boldsymbol{\sigma}, k)$. According to the hypothesis of maximum dissipation, the evolution equations of the plastic flow and the internal variable are respectively derived as

$$-\frac{1}{2}(\mathcal{L}_v \mathbf{b}^e) \cdot (\mathbf{b}^e)^{-1} = \lambda \frac{1}{J} \frac{\partial f}{\partial \boldsymbol{\sigma}}, \quad \dot{\kappa} = \lambda \frac{\partial f}{\partial k}, \quad (5)$$

where $\lambda \geq 0$ is the plastic multiplier. One can note in Eqs.(5) that whereas the evolution of κ is associative, the plastic flow rule is given in the non-associative format. Apart from the theoretical rationality of maximum dissipation, it is common in soil plasticity to introduce the non-associated plastic flow by assuming a plastic potential $g(\boldsymbol{\sigma}, k)$ which is different from the yield function. In this case the derivatives of $f(\boldsymbol{\sigma}, k)$ with respect to $\boldsymbol{\sigma}$ and k in Eqs.(5) are replaced by the ones of $g(\boldsymbol{\sigma}, k)$.

By combining the plastic consistency condition $\dot{f} = 0$ for continuing plastic loading, the rate form of hyperelastic constitutive equation, and the plastic evolution equations (5), the rate form of hyperelasto-plastic constitutive equation can be obtained as

$$\overset{\square}{\boldsymbol{\tau}} = \mathbf{a}^{\text{ep}} : \mathbf{l}, \quad \mathbf{a}^{\text{ep}} = \mathbf{a} - \frac{\left(\mathbf{b} : \frac{1}{J} \frac{\partial \mathbf{g}}{\partial \boldsymbol{\sigma}}\right) \otimes \left(\frac{\partial f}{\partial \boldsymbol{\sigma}} : \frac{1}{J} \mathbf{b}^*\right)}{\frac{\partial f}{\partial \boldsymbol{\sigma}} : \frac{1}{J} \mathbf{b} : \frac{1}{J} \frac{\partial \mathbf{g}}{\partial \boldsymbol{\sigma}} + \frac{\partial f}{\partial k} h \frac{\partial \mathbf{g}}{\partial k}}, \quad (6)$$

where $\overset{\square}{\boldsymbol{\tau}}$ is the nominal rate of the Kirchhoff stress, $h = \partial^2 \Psi / \partial \kappa^2$ is the isotropic hardening modulus, and the fourth-order tensor \mathbf{a}^{ep} is the hyperelasto-plastic tangent modulus. The hyperelastic tangent moduli \mathbf{a} , \mathbf{b} , and \mathbf{b}^* are respectively given as

$$\mathbf{a}_{ijkl} = \mathbf{c}_{ijkl} + \delta_{ik} \tau_{jl}, \quad \mathbf{b}_{ijkl} = \mathbf{c}_{ijkl} + \delta_{ik} \tau_{jl} + \tau_{il} \delta_{jk}, \quad \mathbf{b}_{ijkl}^* = \mathbf{b}_{ijkl} - \tau_{ij} \delta_{kl}, \quad (7)$$

where δ_{ij} is the Kronecker delta. The spatial hyperelastic tangent modulus \mathbf{c} is given by the second derivative of the stored energy function with respect to the relevant elastic deformation tensor. One can note that due to the non-associative format of the flow rule (5)₁, \mathbf{a}^{ep} does not possess major symmetry.

Next, we briefly summarize the formulation for the boundary value problem in finite deformations. The weak form of the quasi-static equilibrium of a domain \mathcal{B} is expressed in the spatial description as

$$\mathcal{I}(\mathbf{u}; \delta \mathbf{u}) = \int_{\varphi(\mathcal{B})} (\delta \mathbf{u} \otimes \nabla_x) : \boldsymbol{\sigma} \, dv - \int_{\partial_t \varphi(\mathcal{B})} \delta \mathbf{u} \cdot \mathbf{t} \, ds = 0, \quad (8)$$

in which body forces are not included. Here $\varphi(\mathcal{B})$ denotes the current configuration of the body \mathcal{B} , $\delta \mathbf{u}$ is an admissible variation of displacement field \mathbf{u} , and \mathbf{t} is the prescribed surface traction on the boundary $\partial_t \varphi(\mathcal{B})$. Under a condition in which configuration-dependent loading is absent, linearization of Eq.(8) with respect to an incremental displacement $\Delta \mathbf{u}$ leads to

$$\mathcal{I} + D\mathcal{I}[\Delta \mathbf{u}] = 0, \quad D\mathcal{I}(\mathbf{u}; \delta \mathbf{u})[\Delta \mathbf{u}] = \int_{\varphi(\mathcal{B})} (\delta \mathbf{u} \otimes \nabla_x) : \frac{1}{J} \mathbf{a}^{\text{ep}} : (\Delta \mathbf{u} \otimes \nabla_x) \, dv. \quad (9)$$

The linearized equation (9) is discretized into the finite-element scheme and, in turn, is to be solved with respect to $\Delta \mathbf{u}$ by iterative scheme. Due to the non-symmetric tangent modulus \mathbf{a}^{ep} , tangent stiffness matrix \mathbf{K} , which is derived by the FE-discretization, is now non-symmetric.

In contrast to the rate formulation for modeling of materials, we should handle discrete increments of finite step sizes in numerical solution procedure for the non-linear equations (9). We thus employ in numerical analyses the exponential return mapping algorithm and the algorithmically consistent tangent operator [1] to ensure the quadratic rate of convergence.

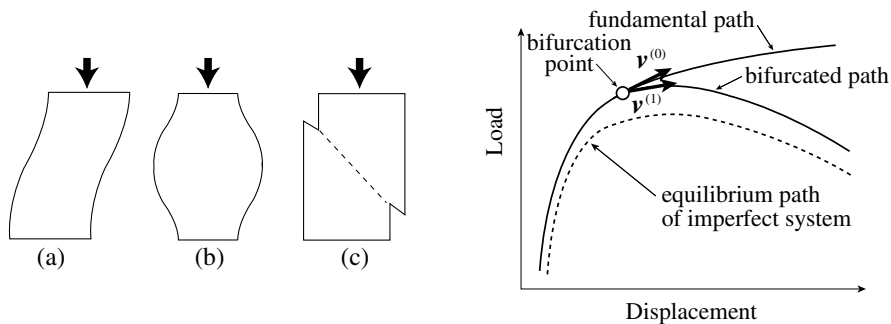


Figure 1. Examples of bifurcation modes. Figure 2. Schematic view of bifurcation.

Detection of Bifurcation and Branch Switching

This section presents numerical procedures for detection of bifurcation and branch switching. We shall limit the discussion to diffuse mode bifurcation ((a) and (b) in Figure 1), which consists of a continuous velocity or velocity gradient field. In this paper, another class of bifurcation, namely, the shear band mode ((c) in Figure 1), is not considered. The bifurcation condition postulated by Hill [3] is expressed in the form

$$\delta I(\mathbf{v}^{(*)}) = \int_{\varphi(\mathcal{B})} (\mathbf{v}^{(*)} \otimes \nabla_{\mathbf{x}}) : \bar{\boldsymbol{\sigma}}^{(*)} dv = 0, \quad (10)$$

where $\bar{\boldsymbol{\sigma}} = \dot{\boldsymbol{\tau}}/J$ denotes the nominal rate of the Cauchy stress. As illustrated in Figure 2, we assume the existence of two distinct solutions of the velocity fields $\mathbf{v}^{(0)}$ and $\mathbf{v}^{(1)}$ at an equilibrium point, and define their difference as $\mathbf{v}^{(*)} = \mathbf{v}^{(1)} - \mathbf{v}^{(0)}$. If non-trivial solution $\mathbf{v}^{(*)} \neq \mathbf{0}$ exists, two distinct solutions $\mathbf{v}^{(0)}$ and $\mathbf{v}^{(1)}$ ($\mathbf{v}^{(0)} \neq \mathbf{v}^{(1)}$) are possible, and a bifurcation point is encountered on the equilibrium path. From Eq.(6), rate constitutive equations for the fields $\mathbf{v}^{(0)}$, $\mathbf{v}^{(1)}$ and the difference of a pair of these equations are

$$\bar{\boldsymbol{\sigma}}^{(0)} = \frac{1}{J} \mathbf{a}^{\text{ep}} : \mathbf{l}^{(0)}, \quad \bar{\boldsymbol{\sigma}}^{(1)} = \frac{1}{J} \mathbf{a}^{\text{ep}} : \mathbf{l}^{(1)} \quad \rightsquigarrow \quad \bar{\boldsymbol{\sigma}}^{(*)} = \frac{1}{J} \mathbf{a}^{\text{ep}} : \mathbf{l}^{(*)} \quad (11)$$

where the differences of $\bar{\boldsymbol{\sigma}}$ and \mathbf{l} are defined as $\bar{\boldsymbol{\sigma}}^{(*)} = \bar{\boldsymbol{\sigma}}^{(1)} - \bar{\boldsymbol{\sigma}}^{(0)}$ and $\mathbf{l}^{(*)} = \mathbf{v}^{(*)} \otimes \nabla_{\mathbf{x}} = \mathbf{l}^{(1)} - \mathbf{l}^{(0)}$, respectively. Substituting Eq.(11) into Eq.(10), and noting the same structure as in Eq.(9), we arrive at vector-matrix form

$$\mathbf{v}^{(*)\text{T}} \mathbf{K} \mathbf{v}^{(*)} = 0 \quad \Rightarrow \quad \mathbf{v}^{(*)} \neq \mathbf{0} \quad \text{if} \quad \det \mathbf{K} = 0 \quad (12)$$

where the notation $\mathbf{v}^{(*)}$ now denotes the vector of the difference of nodal velocities.

The use of the hyperelasto-plastic moduli \mathbf{a}^{ep} in Eq.(11) might be open to criticism, especially when we consider materials which do not obey the associated flow rule. Elasto-plastic bifurcation can be rigorously identified by considering all

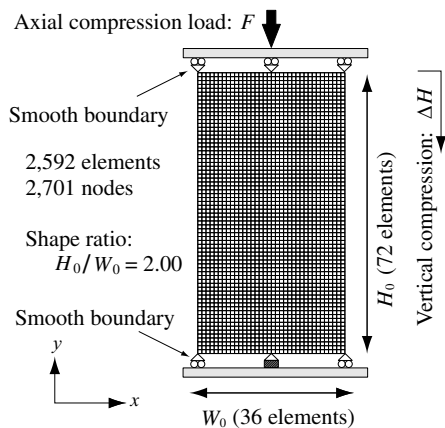


Figure 3. Analysis model.

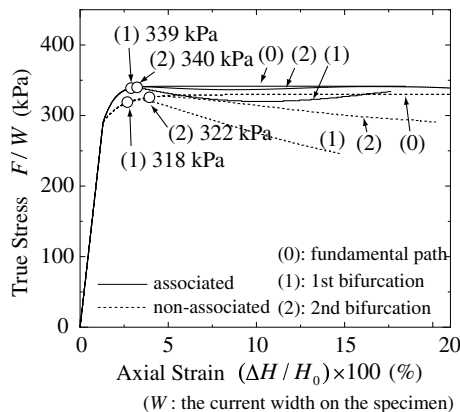


Figure 4. Fundamental and bifurcated paths.

possible combinations of plastic loading and elastic unloading at each point of the domain. In order to examine properly the bifurcation in elasto-plastic materials, the notion of the linear comparison solid by Hill [3] is usually introduced to determine bounds to the range of possible bifurcation. However, the possibility of bifurcation in materials with the non-associated flow rule cannot be necessarily excluded, even though we identify the absence of bifurcation in the comparison solid. Raniecki and Bruhns [4] proposed the generalized notion and the proper choice of comparison solids which can be applicable for non-associative materials.

Once the bifurcation is detected at an equilibrium point, the branch switching is conducted to arrive at the post-bifurcation state by perturbing a homogeneous state with a predictor for the incremental displacement

$$\Delta \mathbf{u}^{(1)} = \Delta \mathbf{u}^{(0)} + \Delta \mathbf{u}^{(*)}, \quad \Delta \mathbf{u}^{(*)} = C \boldsymbol{\theta}, \quad (13)$$

where C is a scaling factor. The increment $\Delta \mathbf{u}^{(1)}$ corresponds to the velocity $\mathbf{v}^{(1)}$ in the rate equations. The bifurcation mode $\boldsymbol{\theta}$ is calculated by means of the method proposed by van der Veen et al. [2]. The Fortran subroutine DGEEV in the LAPACK is utilized in eigen-analysis of non-symmetric tangent stiffness matrix.

Examples of Numerical Bifurcation Analysis

This section presents examples of post-bifurcation analysis. The analyses are conducted for the associated and the non-associated plasticity to examine the effect of plastic flow rule in the behavior of frictional dilatant materials like soils.

Analysis model of the specimen is shown in Figure 3. The Drucker-Prager model without plastic hardening was employed, where the friction angle and the

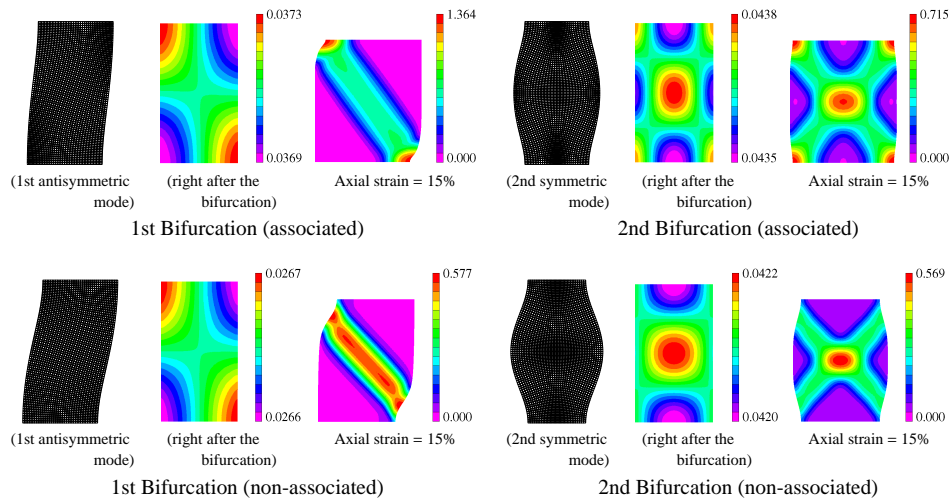


Figure 5. Bifurcation modes (left), post-bifurcation progress of the deformation and the distribution of the shear strain (center and right).

dilatancy angle are set to be 23.5° and 2.0° , respectively. Lamé's constants for hyperelasticity are chosen to be $\lambda = 11.54$ MPa and $\mu = 7.69$ MPa.

The fundamental and bifurcated paths are shown in Figure 4, where the measure of the true stress F/W is employed. One can note from the Figure 4 that the bifurcation stress of the non-associated case is lower than that of the associated case. Figure 5 shows the progress of deformation and the shear strain distribution after the bifurcation. In all cases non-uniform deformation rapidly propagates after the bifurcation, and then gradually concentrates to band-like localized zones.

Reference

1. Meschke, G., Liu, W. N. (1999): "A re-formulation of the exponential algorithm for finite strain plasticity in terms of Cauchy stresses," *Comp. Meth. Appl. Mech. Engrg.*, Vol. 173, pp. 167–187.
2. van der Veen, H., Vuik, K., de Borst, R. (2000): "Branch switching techniques for bifurcation in soil deformation," *Comp. Meth. Appl. Mech. Engrg.*, Vol. 190, pp. 707–719.
3. Hill, R. (1958): "A general theory of uniqueness and stability in elastic-plastic solids," *J. Mech. Phys. Solids*, Vol. 6, pp. 236–249.
4. Raniecki, B., Bruhns, O. T. (1981): "Bounds to bifurcation stresses in solids with non-associated plastic flow law at finite strain," *J. Mech. Phys. Solids*, Vol. 29, No. 2, pp. 153–172.